Chemical Geology 482 (2018) 121–130

Contents lists available at ScienceDirect

Chemical Geology

journal homepage: www.elsevier.com/locate/chemgeo

Cr isotopic composition of the Laobao cherts during the Ediacaran–Cambrian transition in South China

Jing Huang[a,*], Jia Liu[a], Yingnan Zhang[a], Huajin Chang[b], Yanan Shen[a], Fang Huang[a], Liping Qin[a]

[a] CAS Key Laboratory of Crust-Mantle Materials and Environments, School of Earth and Space Sciences, University of Science and Technology of China, Hefei 230026, China

[b] School of Geosciences, Hubei University of Arts and Science, Xiangyang 441053, China

ARTICLE INFO

Editor: Michael E. Böttcher

Keywords:
Cr isotopic composition
Deep water
Ediacaran–Cambrian transition
Chert
Anoxic ocean

ABSTRACT

In this study, we present the Cr isotopic compositions from the cherts in the Laobao Formation (~551–522 Ma) that were deposited in deep water in South China. The Cr concentrations and isotopic compositions in the Laobao cherts were dominated by the contemporaneous seawater and detrital phases. The lower part of the Laobao cherts show that the $\delta^{53}Cr$ of contemporaneous deep seawater in the Huanan basin was approximately −0.1‰, and the $\delta^{53}Cr$ of detrital materials was approximately ≥0.2‰. These findings imply that surface ^{53}Cr-enriched Cr(VI) species did not affect the deep ocean until the late Ediacaran because of the strong redox stratification in the ocean, although the oxidative Cr cycle in terrestrial settings had emerged before that time. A slight rise in $\delta^{53}Cr$ in the deep ocean (to approximately 0.08‰) was estimated for the upper part of the Laobao cherts. If the $\delta^{53}Cr$ rise and its amplitude can be further determined, this will imply that shallow ^{53}Cr-enriched Cr (VI) species had an impact on the deep ocean and will suggest an oxidation of the ocean in the Huanan basin around the Ediacaran–Cambrian boundary (~542 Ma).

1. Introduction

The Ediacaran–Cambrian transition (560–520 Ma) shows the most dramatic biological diversification in Earth's history (Erwin et al., 2011; Marshall, 2006; Zhang and Shu, 2014), and Earth's surface redox condition has been considered a critical trigger for this transition (Chen et al., 2015b; Maloof et al., 2010; Marshall, 2006; Zhang and Shu, 2014). Several lines of evidence suggest the stepwise oxygenation of Earth's surface environment during the Ediacaran (635–542 Ma) and during the middle of the early Cambrian (~520 Ma) (Chen et al., 2015b; Fike et al., 2006; McFadden et al., 2008; Och and Shields-Zhou, 2012; Shen et al., 2008; Wen et al., 2015). However, widespread anoxia and even euxinia (anoxic conditions with free H_2S) were likely present in the deep ocean until at least the earliest Cambrian, and probably into the Ordovician. (Canfield et al., 2008; Feng et al., 2014; Li et al., 2010; Och et al., 2013; Schröder and Grotzinger, 2007; Thompson and Kah, 2012; Wang et al., 2012a; Wen et al., 2015; Wille et al., 2008).

The chromium (Cr) stable isotopic system is an emerging tool for examining the redox conditions of Earth surface environments (Bonnand et al., 2013; Crowe et al., 2013; Frei et al., 2009, 2011, 2013; Gilleaudeau et al., 2016; Planavsky et al., 2014; Qin and Wang, 2017; Reinhard et al., 2014). At the Earth's surface, Cr is predominantly bound in oxides and silicates as Cr(III) within rock-forming minerals. Without oxidation to a higher valence state, it is difficult for Cr(III) dissolved from these minerals to be transported to the ocean owing to its insolubility in water of neutral pH (Fandeur et al., 2009; Frei et al., 2009; Oze et al., 2007; Reinhard et al., 2014). However, in the presence of Mn-oxides that are linked specifically to the presence of free environmental O_2, Cr(III) in soils can be oxidized to highly soluble forms of Cr(VI) (e.g., CrO_4^{2-}, $HCrO_4^-$, $Cr_2O_7^{2-}$) that are readily transported in oxidizing aqueous fluids (Fandeur et al., 2009; Kotaś and Stasicka, 2000; Oze et al., 2007). During subsequent transport processes, Cr(VI) can also be partially reduced to Cr(III) by microbes or by abiotic reductants (e.g. Fe^{2+}, H_2S) and scavenged into Fe(III)–Cr(III) oxyhydroxides (Buerge and Hug, 1997; Eary and Rai, 1989; Fendorf and Li, 1996; Reinhard et al., 2014). Cr (III) oxidation during weathering processes and Cr(VI) reduction during transport processes can generate large kinetic fractionations (6–7‰) and can produce highly mobile Cr (VI) with positive $\delta^{53}Cr$ in aqueous systems (e.g. Frei et al., 2014; Reinhard et al., 2014; Zink et al., 2010). These Cr(VI) species can be transported to the ocean by rivers, and the Cr isotopic composition can be recorded in the marine sediments. Previous studies have indicated that Cr(VI) can be reduced to Cr(III) and then sequestrated into sediments quantitatively when they encounter reductants in the anoxic

* Corresponding author.
E-mail addresses: hjmail@ustc.edu.cn (J. Huang), lpqin@ustc.edu.cn (L. Qin).

https://doi.org/10.1016/j.chemgeo.2018.02.011
Received 21 June 2017; Received in revised form 5 February 2018; Accepted 7 February 2018
Available online 10 February 2018
0009-2541/

ocean (Frei et al., 2009; Reinhard et al., 2014). Cr isotopic fractionation is regarded as negligible in this process; thus, the authigenic Cr in marine sediments such as shales and iron stones can faithfully record the δ^{53}Cr of ambient seawater (Frei et al., 2009; Reinhard et al., 2014). Strongly positive fractionations of Cr isotopes were observed in various ancient marine sediments, suggesting the emergence of extensive Cr oxidation on land at ~780 Ma and possibly even earlier (Frei et al., 2009; Gilleaudeau et al., 2016; Planavsky et al., 2014).

Cr isotopes have been increasingly used to constrain the oxygen level of the ancient atmosphere (Frei et al., 2009; Gilleaudeau et al., 2016; Planavsky et al., 2014), but the application of this method remains limited owing to poor understanding of Cr cycling in the ocean. Recent studies have shown that the Cr isotopes in modern oceans are spatially heterogeneous and depend on the Cr source, the water depth, and redox conditions in the ocean (Bonnand et al., 2013; Reinhard et al., 2014; Scheiderich et al., 2015). Variable Cr isotopic compositions in river water may also play an important role in the δ^{53}Cr of the local seawater (Farkaš et al., 2013; Frei et al., 2014; Paulukat et al., 2015; Rodler et al., 2016).

In this study, we investigated stable Cr isotopic composition in Laobao cherts from the Ediacaran–Cambrian transition system in South China. Laobao cherts are deep-ocean deposits that may have recorded the Cr isotopic composition of contemporaneous deep water and thus could represent Cr isotopic evolution in deep water during the Ediacaran–Cambrian transition. The results may also provide new constraints on the Cr cycling and the redox state change in the ocean at that time.

2. Geological setting

The Yangtze platform developed as a rifted continental margin at the southeastern side of the Yangtze block from ca. 820 Ma and gradually evolved to form a passive continental margin basin during the Ediacaran–Cambrian transition (Jiang et al., 2003; Wang and Li, 2003). The Ediacaran and Cambrian sediments were distributed on this passive continental margin along a paleoseawater depth gradient from the northwest to the southeast in South China (Jiang et al., 2003) (Fig. 1a). During the Ediacaran–Cambrian transition, the lithology of the strata varies depending on the sedimentary facies in South China. In the northwest, the carbonate-predominant (> 100 m thick) Dengying Formation (ca. 551–542 Ma) is overlain by the limestone and phosphorite-interbedded (a few to tens of meters) Kuanchuanpu/Yanjiahe Formation or the Niutitang Formation, which are deposited in shallow water (i.e., the shelf area); in the southeast, the chert-predominant Liuchapo/Laobao/Piyuancun Formation (roughly equivalent to the Dengying Formation) is overlain by the chert, shale, thin mudstone, and phosphorites of Liuchapo or the Niutitang Formation, which are deposited in deep water (i.e., the basinal area) (Zhu et al., 2007). A “transitional zone” characterized by mixed lithology is located in northeastern Guizhou, northern Hunan, and Hubei provinces (Fig. 1a).

The Silikou section is in Silikou village of Sanjiang Dong Autonomous County, northern Guangxi Zhuang Autonomous Region, comprising the upper part of the Ediacaran Doushantuo Formation, the Laobao Formation, and the lower part of the Cambrian Qingxi Formation (Fig. 1b and 2). The lower boundary of the Laobao Formation formed approximately 551 Ma, corresponding to the Dengying–-Doushantuo boundary (Condon et al., 2005), and the upper boundary formed approximately 522 Ma in the early Cambrian (Chen et al., 2015a; Wang et al., 2012c). The new chronology results and stratigraphic correlations suggest that the Ediacaran–Cambrian boundary is in the middle or upper part of the Laobao Formation (Chen et al., 2015a; Hu, 2008; Wang et al., 2012c) (Fig. 2).

The Laobao Formation in the Silikou section is approximately 180 m thick and is mainly characterized by black/grey chert, which was deposited in basin facies (Chang et al., 2012). Below 80 m, the chert is mainly characterized by medium-thick black/grey chert; above 80 m, it is dominated by thin black/grey chert, in which some carbonaceous/siliceous mudstone interbeds are observed (Fig. 2). Most Laobao cherts are finely laminated, and some have a nodular structure and an undulating bedding surface (Chang et al., 2012; Hu, 2008). Many microbolite structures can be distinguished in these cherts: clots/lamellae composed of filamentous algae and stromatolites dominate below ~80 m, and micro-spherites and biofilm structures dominate above 80 m (Hu, 2008). A few potential *protospongia*, acritarchs, and small shell fossils (SSF) were also found in the Laobao cherts (Hu, 2008).

3. Samples and method

All cherts of the Laobao Formation were collected at outcrop as large hand samples to ensure representative sampling and sufficient quantities for the geochemical analyses. Fresh chips of the samples free of weathering surfaces and secondary veins were hand-picked and subsequently ground to powder (< 200 mesh) in an agate mortar to avoid contamination during sample preparation because grinding samples in a steel mortar can introduce Cr contamination.

3.1. Trace elements and rare earth elements (REE)

Approximately 50 mg of each sample powder was weighed and transferred to a Teflon bomb. The samples were dissolved with a three-acid (i.e., HNO_3, HF, and $HClO_4$) digest. The details of this procedure have been described in a previous study (Chang et al., 2012). The samples were then dissolved in 1% HNO_3. The resulting solutions were analyzed for trace elements and REE concentrations using inductively coupled plasma–mass spectrometry (ICP-MS) with In serving as an internal standard; a Finnigan Element system (State Key Laboratory of

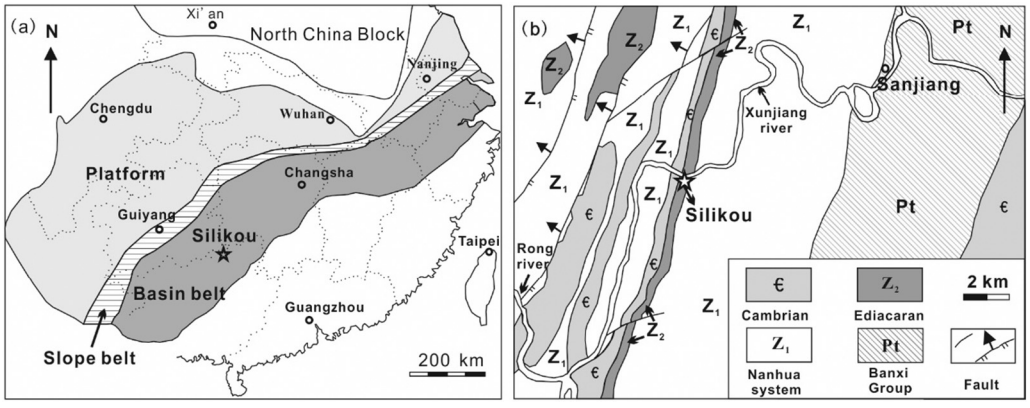

Fig. 1. Study region in the Yangtze Block of South China and geological map of the Silikou section.

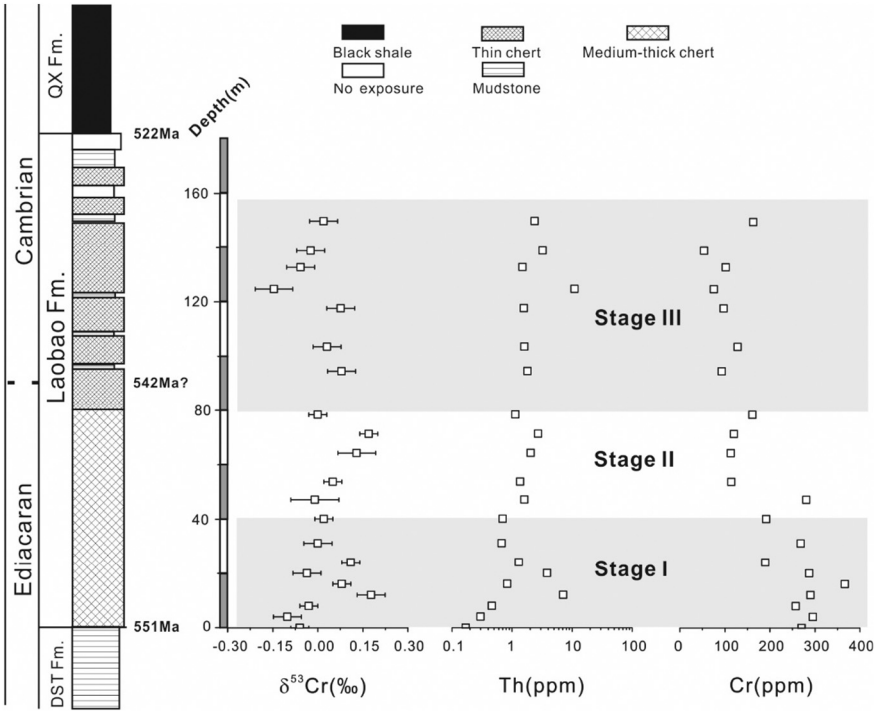

Fig. 2. Stratigraphic column and Cr isotopic composition variations of the Laobao cherts in the Silikou section. Data for the Th concentrations are from Chang et al. (2012).

Lithospheric Evolution, Institute of Geology and Geophysics, Chinese Academy of Sciences, Beijing, China) was used to perform these analyses. The analytical precision monitored by the internal standard is better than 10% (1σ) for trace elements and REE.

3.2. Cr isotopic composition

3.2.1. Sample preparation and chromatography

The chromium isotopic analyses were performed at the Carnegie Institution for Science (Washington, DC) and the University of Science and Technology of China (USTC; Hefei, China). All chemical procedures were performed in a clean laboratory environment. Approximately 10–50 mg rock powder (amounts adjusted to yield 3 μg Cr in the final separate) was attacked by a HF-HNO_3 mixture in closed Savillex beakers on a hot plate at 140 °C for 3–4 days. After being heated to dryness, the residues were reacted with a HCl-HNO_3 mixture in closed Savillex beakers on a hot plate at 140 °C overnight. The samples were then dried, heated, and completely dissolved in 1 ml 6 N HCl. This step was repeated until the samples were completely dissolved. An aliquot of the sample solution containing 1 μg Cr was mixed with 1 ml ^{50}Cr-^{54}Cr double spike (the concentrations of ^{50}Cr and ^{54}Cr were 2.716 nmol/g and 1.742 nmol/g, respectively) and subsequently evaporated to dryness. The details of this double-spike procedure have been reported previously (Han et al., 2012). The sample was then dissolved in 0.2 ml 6 M HCl and heated for 2–3 h at 130 °C before chromatographic separation. The two-step cation exchange chromatography procedure followed a previously described protocol (Qin et al., 2010) in which Bio-Rad 200–400 mesh AG50- × 8 resin was used in both columns. The procedure blanks were approximately 10 ng, which was negligible.

3.2.2. Mass spectrometry and data reproducibility

Ten samples were analyzed using a Thermo Finnigan Triton multi-collector thermal-ionization mass spectrometer (TIMS) at the Carnegie Institution for Science. Details of the mass spectrometry protocol are available in Shen et al. (2015). Eleven samples were analyzed using a Neptune multiple collector ICP-MS (MC-ICP-MS) at the CAS Key Laboratory of Crust-Mantle Materials and Environments at the University of Science and Technology of China (Hefei, China) following an analytical protocol similar to that used for TIMS (Shen et al., 2015). For TIMS, the internal precision [2 standard errors (SE)] on the measured ^{53}Cr/^{52}Cr ratio, based on 14 blocks of 30 ratios at 8 s integration per ratio was typically < 0.03‰. The long-term (over 3 months) reproducibility [± 0.04‰, 2 standard deviations (SD), n = 40] was determined by performing repeated measurements of the spiked National Institute of Standards and Technology (NIST) Standard Reference Material (SRM) 979 standard. For MC-ICP-MS measurements, the long-term precision was better than ± 0.06‰ (n = 103, 2 SD) for the ^{53}Cr/^{52}Cr ratios of the internal standard (SCP). Regardless of which methodology was used, the error assigned to each sample was the largest value among the following: 2 SE of the individual sample, 2 SD of the standard runs obtained in the same session, and the long-term instrumental reproducibility. Some of the Cr solution and geological standards were analyzed by both TIMS and MC-ICP-MS, and the two methods gave identical Cr isotopic results within error limits (Shen et al., 2015). Chromium isotope data are expressed in δ notation, which is the relative deviation of the Cr isotopic ratio in the sample from that in the NIST SRM 979 standard: $\delta^{53}Cr = [(^{53}Cr/^{52}Cr)_{sample}/(^{53}Cr/^{52}Cr)_{SRM979}-1] \times 1000$ (‰).

4. Results

Chromium concentrations and isotopic ratios (δ^{53}Cr) of the samples from the Laobao cherts are listed in Table 1 and are plotted in Fig. 2. Cr concentrations ranged between 54.2 ppm and 366.8 ppm, and δ^{53}Cr values were in a narrow range between −0.15 ± 0.06‰ and 0.18 ± 0.05‰. We divided the Laobao cherts into three stages based on the lithological and geochemical changes. The lower medium-thick black/grey cherts (< 80 m) are Stage I and Stage II, and the upper thin chert (> 80 m) is Stage III (Fig. 2). Previous studies have shown that organic carbon isotope composition and trace element concentrations are more fluctuant below 40 m but are relatively stable between 40 m and 80 m (Hu, 2008; Chang et al. 2012). Thus, 40 m is considered the

Table 1
Chromium isotopic compositions (‰), trace elements and rare earth element concentrations (ppm) from the Laobao cherts in the Silikou section. Data for Th, Zr, and Sc concentrations are from Chang et al. (2012). Some data (eight samples) for TiO_2, Al_2O_3 and REE are from Chang et al. (2010b). $\delta^{53}Cr$ of samples with "*" are measured in Carnegie, and the other samples are measured in USTC.

	SLK-0*	SLK-4	SLK-8*	SLK-12	SLK-16*	SLK-20	SLK-24*
Depth(m)	0.00	4.00	8.00	12.00	16.00	20.00	24.00
$\delta^{53}Cr$(‰)	−0.06	−0.10	−0.03	0.18	0.08	−0.04	0.11
2SD	0.03	0.05	0.03	0.05	0.03	0.05	0.03
Cr	270.30	295.70	257.40	290.30	366.82	287.10	190.20
Zr	10.74	13.18	9.90	12.61	16.19	13.26	27.23
Th	0.17	0.30	0.46	7.10	0.83	3.82	1.30
Sc	0.70	5.40	2.28	9.45	3.41	7.58	6.82
TiO_2 (%)	0.01	0.01	0.02	0.02	0.03	0.02	0.05
Al_2O_3(%)	0.01	0.03	0.17	0.15	0.23	0.24	0.77
La	0.68	1.21	1.21	11.00	1.94	15.05	5.88
Ce	1.07	1.28	1.07	17.34	3.15	18.11	9.02
Pr	0.28	0.36	0.41	2.86	0.50	4.64	1.67
Nd	1.15	1.35	1.67	10.44	1.99	19.46	6.32
Sm	0.30	0.33	0.44	2.31	0.47	4.72	1.25
Eu	0.07	0.09	0.10	0.34	0.10	0.57	0.25
Gd	0.22	0.30	0.53	2.31	0.61	5.06	1.35
Tb	0.03	0.06	0.12	0.43	0.13	0.94	0.26
Dy	0.20	0.42	0.96	3.06	1.13	6.34	1.93
Y	1.61	3.90	7.17	19.34	10.10	37.64	16.82
Ho	0.04	0.11	0.25	0.70	0.30	1.40	0.46
Er	0.14	0.41	0.78	2.22	0.98	4.02	1.46
Tm	0.03	0.07	0.14	0.38	0.17	0.60	0.24
Yb	0.24	0.57	0.92	2.67	1.22	3.87	1.64
Lu	0.05	0.11	0.15	0.43	0.21	0.61	0.27
ΣREE	6.11	10.55	15.92	75.83	23.01	123.04	48.84
Ce/Ce*	0.45	0.39	0.31	0.64	0.72	0.47	0.59
Eu/Eu*	1.34	1.28	0.93	0.69	0.87	0.55	0.90
Y_N/Ho_N	1.48	1.30	1.05	1.01	1.24	0.99	1.34
La/La*	0.58	0.77	0.70	0.87	0.91	0.78	0.81
Pr_N/Sm_N	0.59	0.69	0.59	0.78	0.67	0.62	0.84
Sm_N/Yb_N	0.64	0.29	0.24	0.44	0.20	0.62	0.39
Pr_N/Yb_N	0.37	0.20	0.14	0.34	0.13	0.38	0.33

	SLK-31	SLK-40*	SLK-47*	SLK-53.5*	SLK64*	SLK-71*	SLK-78*
Depth(m)	31.00	40.00	47.00	53.50	64.00	71.00	78.00
$\delta^{53}Cr$(‰)	0.00	0.02	−0.01	0.05	0.13	0.17	0.00
2SD	0.05	0.03	0.08	0.03	0.06	0.03	0.03
Cr	268.80	191.80	281.20	114.10	113.20	120.20	161.50
Zr	20.46	15.88	30.27	24.07	28.27	43.05	23.51
Th	0.67	0.70	1.60	1.37	2.04	2.72	1.14
Sc	3.58	5.85	4.94	6.80	7.27	7.85	4.81
TiO_2 (%)	0.03	0.04	0.14	0.1	0.13	0.2	0.09
Al_2O_3(%)	0.33	0.73	1.3	1.39	2	0.67	1.32
La	5.89	5.83	9.31	9.55	11.36	14.33	7.57
Ce	11.55	8.51	10.98	11.35	15.49	18.53	9.23
Pr	1.85	1.59	2.08	2.01	2.74	3.28	1.59
Nd	7.81	5.92	6.81	6.67	8.85	12.33	4.96
Sm	1.99	1.11	1.08	1.17	1.38	2.21	0.91
Eu	0.51	0.22	0.22	0.28	0.21	0.46	0.22
Gd	2.31	1.04	0.83	1.03	0.89	1.90	0.72
Tb	0.41	0.19	0.14	0.17	0.14	0.33	0.13
Dy	2.70	1.30	0.98	1.10	0.80	2.15	0.84
Y	20.68	11.10	8.66	9.47	5.71	16.03	6.66
Ho	0.60	0.31	0.24	0.25	0.18	0.50	0.20
Er	1.75	0.98	0.78	0.81	0.60	1.57	0.70
Tm	0.27	0.17	0.14	0.14	0.11	0.26	0.12
Yb	1.87	1.13	0.98	1.05	0.83	1.79	0.87
Lu	0.32	0.18	0.16	0.17	0.13	0.28	0.14
ΣREE	60.51	39.57	43.37	45.24	49.42	75.94	34.86
Ce/Ce*	0.76	0.58	0.50	0.54	0.53	0.61	0.52
Eu/Eu*	1.16	0.95	1.07	1.21	0.87	1.05	1.23
Y_N/Ho_N	1.27	1.31	1.32	1.39	1.16	1.18	1.22
La/La*	0.77	0.83	0.96	1.02	0.88	1.00	0.99
Pr_N/Sm_N	0.58	0.90	1.21	1.08	1.25	0.93	1.10
Sm_N/Yb_N	0.54	0.50	0.56	0.57	0.84	0.63	0.53
Pr_N/Yb_N	0.32	0.45	0.68	0.61	1.05	0.59	0.58

(*continued on next page*)

Table 1 (*continued*)

	SLK-94	SLK-103	SLK-117	SLK124	SLK-132	SLK-138	SLK-149
Depth (m)	94.00	103.00	117.00	124.00	132.00	138.00	149.00
δ^{53}Cr(‰)	0.08	0.03	0.08	−0.15	−0.06	−0.02	0.02
2SD	0.05	0.05	0.05	0.06	0.05	0.05	0.05
Cr	93.00	128.20	97.50	75.40	102.10	54.20	77.80
Zr	28.87	29.05	28.06	151.85	25.54	49.19	35.24
Th	1.82	1.61	1.57	11.03	1.50	3.23	2.39
Sc	8.19	6.82	4.80	25.03	5.26	8.93	3.20
TiO_2 (%)	0.13	0.14	0.13	0.86	0.09	0.19	0.12
Al_2O_3(%)	1.97	1.79	2012	14.73	1.85	4.92	2.46
La	6.18	10.41	8.65	34.76	5.59	14.25	9.40
Ce	7.95	12.73	10.54	50.22	8.36	22.61	11.25
Pr	1.42	2.09	1.67	6.80	1.19	2.87	1.94
Nd	4.50	6.48	5.74	21.44	3.93	9.28	7.27
Sm	0.78	0.98	1.00	3.04	0.69	1.45	1.62
Eu	0.18	0.19	0.15	0.64	0.11	0.20	0.32
Gd	0.36	0.48	0.58	1.90	0.29	0.72	1.49
Tb	0.05	0.08	0.09	0.30	0.05	0.12	0.25
Dy	0.33	0.58	0.60	1.99	0.34	0.78	1.43
Y	3.30	5.73	4.98	12.41	2.72	5.22	8.40
Ho	0.08	0.16	0.14	0.46	0.08	0.18	0.28
Er	0.28	0.51	0.46	1.53	0.27	0.55	0.77
Tm	0.05	0.09	0.08	0.27	0.04	0.09	0.12
Yb	0.40	0.67	0.58	1.98	0.32	0.61	0.76
Lu	0.07	0.12	0.10	0.34	0.05	0.10	0.12
ΣREE	25.92	41.30	35.35	138.08	24.02	59.02	45.40
Ce/Ce*	0.51	0.55	0.63	0.67	0.67	0.74	0.63
Eu/Eu*	1.54	1.19	0.89	1.21	1.02	0.84	0.98
Y_N/Ho_N	1.51	1.31	1.31	0.99	1.25	1.06	1.10
La/La*	0.91	1.03	1.13	1.07	1.01	1.05	1.11
Pr_N/Sm_N	1.14	1.34	1.05	1.41	1.08	1.24	0.75
Sm_N/Yb_N	0.99	0.74	0.88	0.78	1.10	1.21	1.08
Pr_N/Yb_N	1.13	1.00	0.92	1.10	1.19	1.50	0.82

boundary between Stage I and Stage II (Fig. 2). The stratigraphic change of δ^{53}Cr and Th contents show similar trends below 80 m (Stage I and II): Both show a trend of increasing below 20 m, decreasing from 20 m to 40 m, and then increasing from 40 m to 80 m. They show different trends above 80 m (Stage III): δ^{53}Cr shows a trend of decreasing from 80 m to 120 m and then increasing above 120 m, whereas Th shows a trend of increasing from 80 m to 120 m and then decreasing above 120 m.

REE anomalies are calculated using the following formulae: $Ce/Ce^* = Ce_N / [Pr_N \times (Pr_N/Nd_N)]$; $Eu/Eu^* = Eu_N / (Sm_N^2 \times Tb_N)^{1/3}$; $La/La^* = La_N / [Pr_N \times (Pr_N/Nd_N)^2]$ (Lawrence et al., 2006). Concentrations of elements with the subscript N have been normalized to Post-Archaean Australian Shale (PAAS) (McLennan, 1989). Within Stage I, total REE contents ranged between 6.1 ppm and 123.0 ppm, with moderately negative Ce anomalies ($Ce/Ce^* = 0.55 \pm 0.15$), slightly positive Y anomalies ($Y_N/Ho_N = 1.22 \pm 0.17$), no distinct positive Eu anomalies ($Eu/Eu^* = 0.96 \pm 0.26$), and light REE (LREE) depletion and heavy REE (HREE) enrichment ($Pr_N/Sm_N = 0.69 \pm 0.12$, $Sm_N/Yb_N = 0.43 \pm 0.16$, $Pr_N/Yb_N = 0.30 \pm 0.11$). Within Stage II, total REE contents ranged between 34.9 ppm and 75.9 ppm, with moderately negative Ce anomalies ($Ce/Ce^* = 0.54 \pm 0.04$), slightly positive Y anomalies ($Y_N/Ho_N = 1.26 \pm 0.10$), no distinct positive Eu anomalies ($Eu/Eu^* = 1.09 \pm 0.15$), and slight LREE depletion and HREE enrichment ($Pr_N/Sm_N = 1.11 \pm 0.12$, $Sm_N/Yb_N = 0.63 \pm 0.13$, $Pr_N/Yb_N = 0.70 \pm 0.20$). Within Stage III, total REE contents ranged between 24.0 ppm and 138.1 ppm, with moderately negative Ce anomalies ($Ce/Ce^* = 0.63 \pm 0.08$), slightly positive Y anomalies ($Y_N/Ho_N = 1.22 \pm 0.18$), no distinct positive Eu anomalies ($Eu/Eu^* = 1.10 \pm 0.24$), and no LREE depletion or HREE enrichment ($Pr_N/Sm_N = 1.15 \pm 0.22$, $Sm_N/Yb_N = 0.97 \pm 0.17$, $Pr_N/Yb_N = 1.09 \pm 0.22$).

5. Discussion

5.1. Sources of Cr in the Laobao cherts

Previous study showed that framboidal pyrites were common in the Laobao cherts; these pyrites have small diameters (mostly < 7 μm) and a narrow size range (the maximum diameters range from 7.7 μm to 18 μm) (Wilkin et al., 1996, 1997). The small sizes and narrow size range of framboidal pyrites indicate that they formed in the water column because their sizes were limited by the fast reaction rate and unstable water dynamic conditions (Wilkin et al., 1996, 1997). This finding further suggests either that the seawater was euxinic or that sulfate reduction occurred in the seawater, both of which indicate an anoxic depositional condition (Chang et al., 2009, 2012). High enrichments in redox-sensitive trace elements (U, V, Mo), very low Th/U ratios (< 2), high V/Sc (> 7.9) ratios, and high V/(V + Ni) (> 0.6) ratios were found in the Laobao cherts, also indicating that these cherts were deposited under anoxic conditions (Chang et al., 2012). In addition, the high reactive iron ratios (FeHR/FeT > 0.38) in the Laobao cherts support anoxic conditions (Chang et al., 2010a). The Laobao cherts show moderately negative Ce-anomalies (Fig. 3 and Table 1), but this does not necessarily argue against the anoxic-conditions scenario. The strongly anoxic deep water in the Black Sea also shows moderately to slightly negative Ce-anomalies (0.4–1.0; mostly 0.8) (German et al., 1991; Schijf et al., 1991), and high contents of authigenic phosphate and Fe-rich smectite may play a role in the negative Ce-anomaly in sediments as well (Pattan et al., 2005).

As discussed previously, the δ^{53}Cr of authigenic Cr in shales and iron-rich marine chemical sediments can represent the Cr isotope composition of ambient seawater because of the quantitative Cr(VI) reduction and subsequent sequestration into the sediments that occurs under anoxic conditions (Frei et al., 2009; Reinhard et al., 2014). In

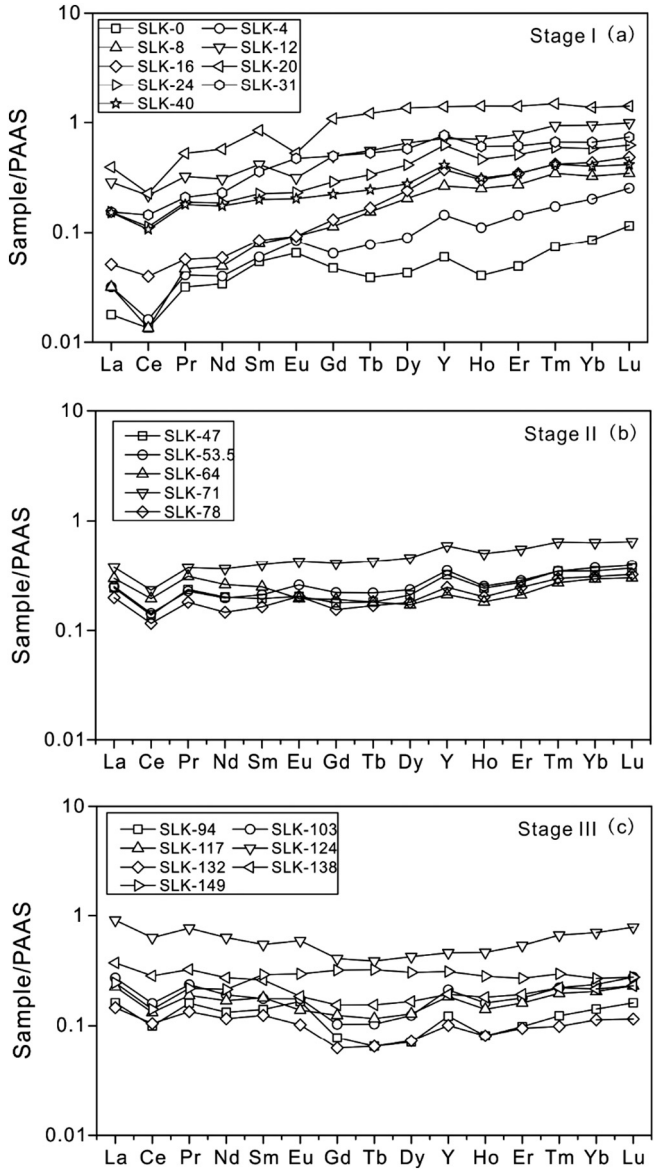

Fig. 3. REE + Y patterns of the Laobao cherts in the Silikou section
Some data (eight samples) are from Chang et al. (2010b).

terms of how Cr was incorporated into the Laobao cherts, Cr(III) may be adsorbed to primary silica gels. No published data on Cr isotope fractionation during Cr(III) adsorption are available. However, a previous study indicated that the Cr(III) phases were mostly adsorbed on silica as $Cr(OH)^{2+}$, $Cr(OH)_2{}^{+}$, and $Cr(OH)_3$(aq), and complete (100%) Cr(III) sorption would occur at pH ≥ 6 (Fendorf et al., 1994). This finding implies that the adsorption is quantitative by silica gels under neutral conditions, which is indicated by high Cr concentrations in the Laobao cherts. Therefore, there is no fractionation as Cr(III) incorporates into the cherts under anoxic conditions, and the authigenic Cr in the Laobao cherts can be used to trace the Cr isotope composition of the contemporaneous seawater.

Hydrothermal systems may provide an alternative source of Cr in seawater, which was speculated to have low δ^{53}Cr values (close to those of the primary igneous rocks) and high Cr concentrations (Bonnand et al., 2013; Holmden et al., 2016; Planavsky et al., 2014; Sander and Koschinsky, 2000; Wang et al., 2016). If the Laobao cherts deposited near a zone of significant hydrothermal discharge or experienced hydrothermal postalternation, the δ^{53}Cr would be overprinted by the hydrothermal signals. Positive Eu concentration anomalies in seawater are always associated with hydrothermal fluids (Edmonds and German, 2004); thus, the lack of positive Eu anomalies in the Laobao cherts can exclude local hydrothermal overprint and hydrothermal postalternation (Fig. 3). However, these cannot exclude remote hydrothermal contributions to the deep ocean because REE are usually confined to places near hydrothermal activity by continuous extraction from seawater during hydrothermal precipitate dispersal (German et al., 1990). The Laobao cherts recorded the information of deep seawater, which likely had received and homogenized hydrothermal input Cr elsewhere. Previous work has shown that the hydrothermal activity during the Ediacaran–Cambrian transition mainly occurred on the carbonate platform margin in the Huanan basin (Chen et al., 2009; Fan et al., 2013; Wang et al., 2012b), which would introduce hydrothermal Cr to the Huanan basin, but no positive Eu anomalies were observed in the distant deep basinal seawater.

Diagenetic or metamorphic processes can result in alterations of Cr concentrations and δ^{53}Cr in sediments (Planavsky et al., 2014; Rodler et al., 2016; Wang et al., 2016). The formation mechanism for the cherts is complicated, but the existing evidence supports that the Laobao cherts were directly deposited from seawater: (1) The Laobao cherts have finely laminated fabric, numerous microbolite structures (e.g., filamentous algae, stromatolites, microspherites and biofilm structures), and a few potential fossils (potential *protospongia,* acritarch, and SSF), showing the primary sedimentary structures without strong diagenesis or replacement (Chang et al., 2012; Hu, 2008; Dong et al., 2015); (2) the small size and narrow size range of framboidal pyrites indicate that they formed in the water column (Chang et al., 2009); (3) the Ge/Si ratio of the dominant quartz component in the Laobao cherts was estimated to be 0.4–0.5 μmol/mol, which is close to those of modern seawater and biogenic silica (Dong et al., 2015); (4) the REE + Y patterns show typical seawater features within Stages I and II and more detrital silicate features within Stage III. In addition, the lack of obvious positive Eu anomalies can exclude hydrothermal postalteration; the H/C atomic ratio of kerogen indicates that the cherts experienced little thermal alteration (Hu, 2008). Therefore, the Laobao cherts recorded the primary seawater information and did not undergo a strong diagenesis, metasomatism, or recrystallization.

Detrital Cr phases may contribute significant Cr in sedimentary rocks, which is likely to overprint the Cr isotope signature in the seawater. Some incompatible elements and high-field-strength elements (HFSEs) (e.g., Zr, Th, Ti, Sc) have commonly been used to evaluate detrital contributions (Böning et al., 2004; Schröder and Grotzinger, 2007). Compared with average shales, most of the Laobao cherts contain low concentrations of Zr, Th, Ti, and Sc (Table 1), suggesting minor detrital contributions. Fig. 4a shows no positive correlation between Th and Cr concentrations, and there is a roughly negative correlation between them. This finding indicates that the authigenic phase has much more Cr than the detrital phases, and the Cr concentrations would be diluted by the detrital phases. Fig. 4b shows a positive correlation between Th and δ^{53}Cr within Stages I and II, implying that more detrital phases would cause higher δ^{53}Cr in the cherts. Similarly, the negative correlation within Stage III implies that more detrital phases would cause lower δ^{53}Cr in the cherts. These observations further suggest that the δ^{53}Cr value in the detrital phases is relatively high within Stages I and II, but low within Stage III.

5.2. Cr isotopic compositions from contemporaneous seawater and detrital phases

As discussed above, the Cr concentrations and isotopic compositions in the Laobao cherts are dominated by authigenic Cr, with minor detrital input. Thus, Cr in the Laobao cherts can be considered a mixture of these two sources. In addition, the authigenic Cr in the Laobao cherts can be used to trace the Cr isotope composition of the contemporaneous seawater under anoxic conditions. Therefore, the Cr isotopic composition in the cherts ($\delta^{53}Cr_c$) can be defined by the following equation:

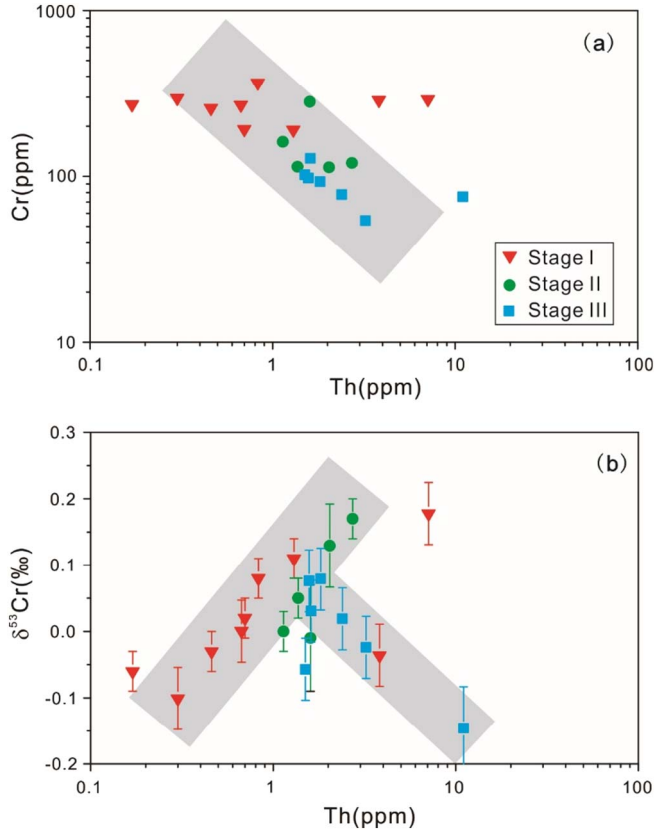

Fig. 4. Plot of Cr concentrations and Cr isotopic compositions versus Th concentrations in the Laobao cherts from the Silikou section.

$$\delta^{53}Cr_c = (1-f)\times\delta^{53}Cr_s + f\times\delta^{53}Cr_d = \delta^{53}Cr_s + f\times(\delta^{53}Cr_d - \delta^{53}Cr_s), \quad (1)$$

where $\delta^{53}Cr_s$ and $\delta^{53}Cr_d$ represent the Cr isotopic composition in contemporaneous seawater and in the detrital phases, respectively, and f represents the mass proportion of Cr in the detrital phases ($M_{Cr\text{-}d}$) to the total Cr in the cherts (M_{Cr}); that is, $f = M_{Cr\text{-}d}/M_{Cr}$

Th is used as the monitor for detrital input in the present study. As an incompatible element that is scarcely derived from seawater, the mass of detrital Th ($M_{Th\text{-}d}$) is equal to the total Th mass (M_{Th}) in the cherts. Therefore, f can be written in the following form:

$$f = (M_{Cr\text{-}d}/M_{Th})\times(M_{Th}/M_{Cr}) = (M_{Cr\text{-}d}/M_{Th\text{-}d})\times(M_{Th}/M_{Cr}), \quad (2)$$

and the Cr isotopic composition of the cherts can be represented as follows:

$$\begin{aligned}\delta^{53}Cr_c &= \delta^{53}Cr_s + (M_{Cr\text{-}d}/M_{Th\text{-}d})\times(M_{Th}/M_{Cr})\times(\delta^{53}Cr_d - \delta^{53}Cr_s)\\ &= \delta^{53}Cr_s + (C_{Cr\text{-}d}/C_{Th\text{-}d})\times(\delta^{53}Cr_d - \delta^{53}Cr_s)\times(C_{Th}/C_{Cr}),\end{aligned} \quad (3)$$

where $C_{Cr\text{-}d}$ and $C_{Th\text{-}d}$ represent the concentrations of Cr and Th, respectively, in the detrital phases, and C_{Th} and C_{Cr} represent the concentrations of Th and Cr, respectively, in the cherts.

If the sources of the detrital Cr and the seawater Cr remained constant during a given geological time, both $\delta^{53}Cr_s$ and $(C_{Cr\text{-}d}/C_{Th\text{-}d})\times(\delta^{53}Cr_d - \delta^{53}Cr_s)$ should be constant. Then, a linear correlation is expected between $\delta^{53}Cr_c$ and C_{Th}/C_{Cr}, where the y-intercept of the line represents $\delta^{53}Cr_s$, and the slope corresponds to $(C_{Cr\text{-}d}/C_{Th\text{-}d})\times(\delta^{53}Cr_d - \delta^{53}Cr_s)$. Most of the samples from Stages I and II fall on their respective positive linear trends (with different slopes) in the $\delta^{53}Cr_c$–C_{Th}/C_{Cr} space (Fig. 5a), whereas most Stage III samples form a negative linear correlation (Fig. 5b). These relatively well-defined linear correlations suggest that the composition of the detrital input and seawater were roughly unchanged within the individual stages. There are a few exceptions within Stages I and III (Fig. 5a and b), which can be explained by temporary perturbations in the seawater or in the detrital input (e.g., short-term changes in detrital source or ocean ventilation).

The y-intercepts of the correlation lines suggest that the $\delta^{53}Cr$ values of contemporaneous seawater ($\delta^{53}Cr_s$) were approximately -0.09 ± 0.02‰ and -0.08 ± 0.04‰ within Stages I and II, respectively. The approximate $\delta^{53}Cr$ of the seawater is consistent with many banded iron formation (BIF)/iron-enriched chert records before the Neoproterozoic (Frei et al., 2009; Planavsky et al., 2014). A recent study reported the authigenic Cr isotopic compositions (between -0.69‰ and 0.02‰) in the Ediacaran cap carbonate, in which the carbonate deposited in deep water showed authigenic $\delta^{53}Cr$ ranging between -0.11‰ and 0.02‰ (Rodler et al., 2016). The low $\delta^{53}Cr$ values in the initial Ediacaran deep ocean are similar to our result during the terminal Ediacaran.

To satisfy the observed $\delta^{53}Cr$ range in our samples and two end-members mixing model, the detrital phases must have positive $\delta^{53}Cr$ values $\geq\sim0.15$‰ within Stage I and $\geq\sim0.20$‰ within Stage II (Fig. 5a). Many studies considered the $\delta^{53}Cr$ of detrital phases in sediments equal to the mean $\delta^{53}Cr$ value for bulk silicate Earth (BSE) (-0.124 ± 0.101‰) (Gilleaudeau et al., 2016; Gueguen et al., 2016; Rodler et al., 2016), but the major change in Cr cycling had occurred before 750 Ma and even earlier, when many ^{53}Cr-enriched ($\delta^{53}Cr > 1$‰) sediments (e.g., shales, carbonates, iron stones) had been documented (Gilleaudeau et al., 2016; Planavsky et al., 2014). In addition, the sediment weathering profiles likely hold positive $\delta^{53}Cr$ because a significant proportion of the released ^{53}Cr-enriched mobile Cr (VI) is immobilized near the weathering surface owing to reduction or adsorption during oxidative weathering (Frei et al., 2014; Wang et al., 2016). These ^{53}Cr-enriched sediments and associated weathering profiles would also be viable detrital sources for the marine sediments. Reinhard et al. (2014) used the average bulk isotope composition of the underlying oxic sediments ($\delta^{53}Cr = 0.13$‰) as the detrital $\delta^{53}Cr$ of sediments in Cariaco Basin, which is close to the detrital estimation for the Laobao cherts within Stages I and II.

Within Stage III, the y-intercepts of the correlation lines suggest that the $\delta^{53}Cr$ of contemporaneous seawater ($\delta^{53}Cr_s$) was approximately 0.08 ± 0.03‰ (Fig. 5b). To satisfy the observed trend in Fig. 5b, the detrital phases must have negative $\delta^{53}Cr$ values $\leq\sim-0.1$‰. Most igneous rocks and ^{53}Cr-depleted sediments meet this requirement (Frei et al., 2014; Schoenberg et al., 2008; Wang et al., 2016). Detrital-authigenic mixing trends suggest a change in the $\delta^{53}Cr$ of detrital material from Stages I/II to Stage III, which can potentially be explained by a shift in provenance from a recycled sedimentary source with a positive $\delta^{53}Cr$ to an igneous source with the crustal $\delta^{53}Cr$. From Stage II to Stage III, the Pr_N/Yb_N ratio changes from 0.70 ± 0.20 to 1.09 ± 0.22 (Table 1), suggesting a LREE/HREE ratio change. Furthermore, the appearance of carbonaceous/siliceous mudstone interbeds within Stage III indicates that the sediments were more influenced by detrital materials than those from the previous stages. Taken together, these findings all support the potential detrital provenance change between Stage II and Stage III.

Our conclusion can also be validated by using Ti instead of Th as the detrital proxy (Fig. 5c and d).

5.3. $\delta^{53}Cr$ evolution and its redox implication of the deep ocean in the Huanan basin during the Ediacaran–Cambrian transition

Samples from previous studies show positive $\delta^{53}Cr$ values (up to 4.90‰) in Neoproterozoic sediments (Frei et al., 2009, 2013; Planavsky et al., 2014). However, these previously analyzed samples all seem to have been deposited in relatively shallow water. For example, the Wynniatt Formation shales were described as the subtidal and peritidal facies sediments (Planavsky et al., 2014), and the carbonate and iron-rich chemical sediments in the Arroyo del Soldado Group (ASG) represent the marine platform successions (Frei et al., 2011, 2013).

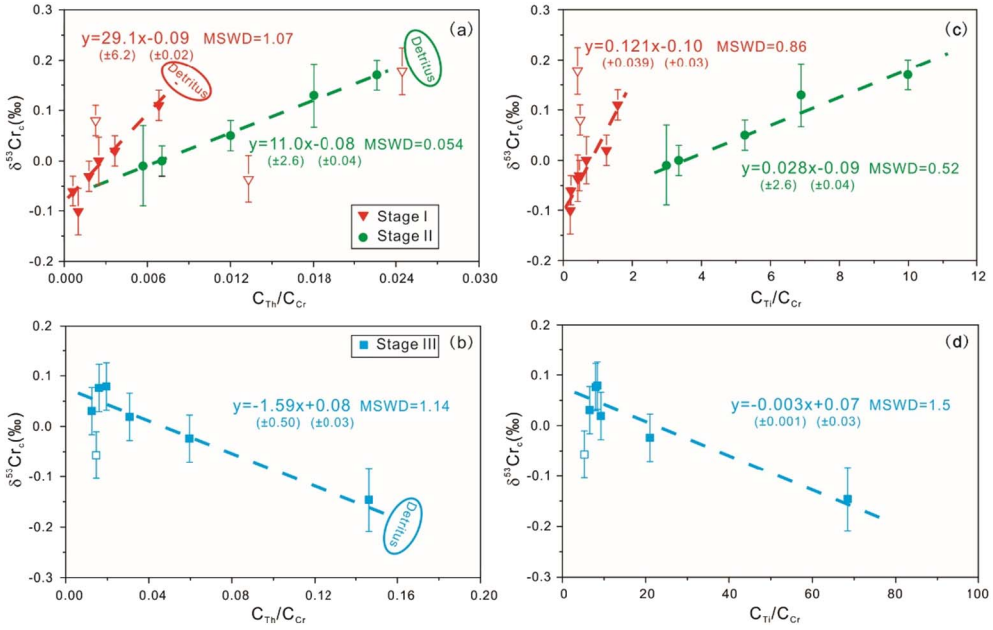

Fig. 5. Plot of Cr isotopic compositions ($\delta^{53}Cr_c$) versus C_{Th}/C_{Cr} ratios and C_{Ti}/C_{Cr} ratios for the Laobao cherts from the Silikou section. The hollow sample points are not used to regress linear equations because they do not follow the premise that the detrital input and the seawater were invariable. The errors of the slopes and *y*-intercepts in the regression lines were calculated by taking the given precisions of the $\delta^{53}Cr$ and element contents.

Therefore, positive Cr-isotope values during the Ediacaran are only definitively recorded in shallow water up to now.

Rodler et al. (2016) examined cap carbonates deposited in basin facies and found mostly low authigenic $\delta^{53}Cr$ values (between −0.11‰ and 0.02‰), suggesting unfractionated Cr in the deep ocean during the initial Ediacaran (ca. 635 Ma). Our $\delta^{53}Cr$ in Stages I and II also show unfractionated values, indicating that the deep oceans were characterized by isotopically unfractionated Cr during the late Ediacaran (ca. 551–542 Ma). We then see a slight shift towards positive $\delta^{53}Cr$ values in deep-water cherts across the Ediacaran–Cambrian boundary (ca. 542 Ma), consistent with positively fractionated Cr in slope/basin shales of the early Cambrian (Lehmann et al., 2016).

Cr isotopic compositions are spatially heterogeneous in modern oceans (Bonnand et al., 2013; Reinhard et al., 2014; Scheiderich et al., 2015), where there is a strong correlation between $\delta^{53}Cr$ and Cr concentration (Scheiderich et al., 2015). Cr(VI) can be partially reduced in surface waters and oxygen minimum zones, generating isotopically light Cr(III) that is scavenged to deep water or to underlying sediments. This isotopic fractionation was estimated to be −0.80 ± 0.03‰, and the ^{53}Cr-depleted Cr(III) can subsequently be released back into seawater by organic complexation or reoxidation (Scheiderich et al., 2015). This process can make the $\delta^{53}Cr$ of modern deep seawater as low as 0.31‰ (Paulukat et al., 2016). However, this mechanism cannot be applied to the Ediacaran ocean, which is strongly stratified with anoxic deep water (Canfield et al., 2008; Chang et al., 2012; Feng et al., 2014; Li et al., 2010; Och et al., 2013; Schröder and Grotzinger, 2007; Wang et al., 2012a; Wen et al., 2015; Wille et al., 2008). The reduction of Cr (VI) likely occurred near the chemocline, but most Cr(III) would be removed and little could be reoxidized and released back into seawater in the deep anoxic ocean.

Cr in the deep ocean during the terminal Ediacaran may come from three sources: (1) inherited from early seawater; (2) hydrothermal input; (3) surface water input (Fig. 6a). Before the emergence of extensive terrestrial Cr oxidation, Cr input into the ocean might have depended on hydrothermal flux and potential terrestrial weathering by biogenic acids; both of these sources supplied Cr(III) (Crowe et al., 2013; Frei et al., 2009; Konhauser et al., 2011). Thus, the early ocean had $\delta^{53}Cr$ close to the igneous sources, and these low values were sustained in the deep ocean until the Ediacaran (Frei et al., 2009; Konhauser et al., 2011; Rodler et al., 2016). The hydrothermal input Cr also had low $\delta^{53}Cr$ values. When the oxidation of Cr was activated on

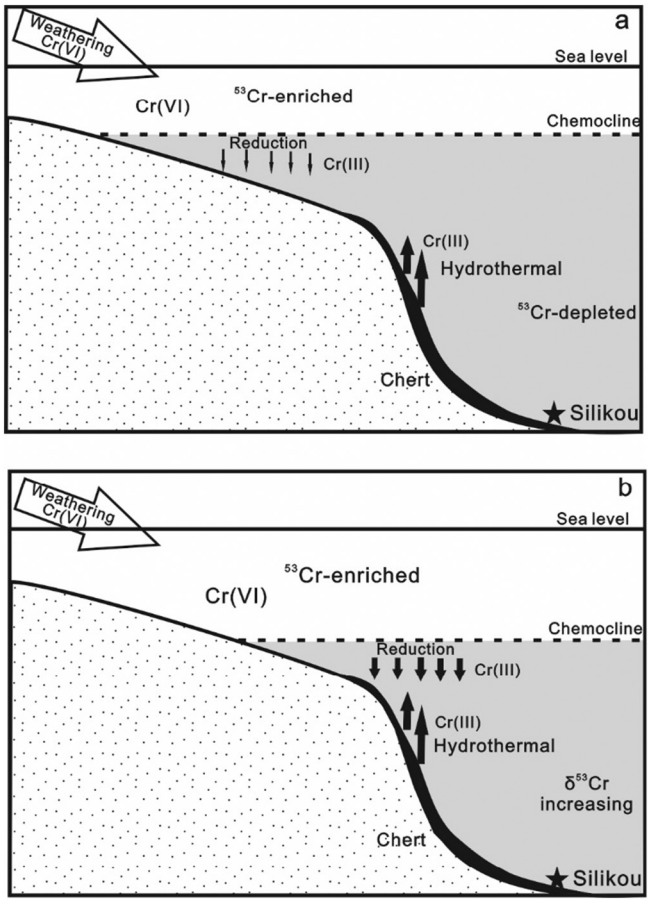

Fig. 6. Schematic representation of the Cr isotopic compositions in the deep ocean of the Huanan basin during the Ediacaran–Cambrian transition period. a. Within Stages I and II, the deep ocean was dominated by the inherited Cr from early seawater and the hydrothermal input Cr, and the surface ^{53}Cr-enriched Cr(VI) species could not affect the deep water. b. Within Stage III, the deepening of the chemocline might reduce the barrier of anoxia, and higher Cr(VI) concentration in the surface water might increase the Cr downward input, both of which could enhance the influence of the surface water on the deep water and increase the $\delta^{53}Cr$ in the deep water.

land, ^{53}Cr-enriched Cr(VI) species could be transported into the surface ocean and then attempt to migrate to the deep ocean. However, under widespread anoxic conditions, the Cr(VI) species would be reduced to Cr(III) near the chemocline and would be quantitatively removed from the seawater before reaching the deep ocean (Fig. 6a). In addition, little of the removed Cr(III) could be released back into seawater by reoxidation under such anoxic conditions. Thus, the ^{53}Cr-depleted pool and the widespread anoxia maintained the low δ^{53}Cr in the deep ocean until the terminal Ediacaran (Fig. 6a).

The δ^{53}Cr value of seawater within Stage III seems to be slightly higher than that of the previous stage (from −0.1‰ to 0.08‰). More work is needed to evaluate this δ^{53}Cr rise; if it can be confirmed within Stage III, it may imply an oxidation of the ocean in the Huanan basin around the Ediacaran–Cambrian boundary. An increase in the δ^{53}Cr of deep water suggests enhanced ^{53}Cr-enriched influences from the surface water, which may be attributed to the following: (1) a deepening of the chemocline, which would reduce/remove the barrier of anoxia (Fig. 6b); (2) an increase of the Cr concentration in the surface water that may enhance the downward input through diffusion (Fig. 6b); (3) an oceanic ventilation change that would deliver more shallow Cr into the deep ocean by inflow. Deepening of the chemocline and an increase of the Cr concentration in the surface water may be related to changes in the redox state of the atmosphere and the ocean; oceanic ventilation change can force more surface oxic water to enter the deep water, which would also result in oxidation of the deep anoxic water to some extent. δ^{53}Cr values in the deep ocean are significantly positive in the Huanan basin during the early Cambrian (Lehmann et al., 2016), suggesting the prominent atmosphere/ocean oxidation that is also consistent with Mo isotope research (Chen et al., 2015b). If the deep ocean oxidation and δ^{53}Cr rise were progressive during the early Cambrian, they were very likely activated around the Ediacaran–Cambrian boundary.

6. Conclusion

Variations of the Cr isotopic composition in the Laobao cherts reflect those in the contemporaneous seawater as well as the detrital input in the Huanan basin during the Ediacaran-Cambrian transition. Within Stages I and II (below 80 m), the δ^{53}Cr of contemporaneous deep water was as low as those of the igneous sources (~ -0.1‰), and the detrital phases show relatively high δ^{53}Cr values (approximately $\geq \sim 0.2$‰) that may have been derived from ^{53}Cr-enriched recycled sediments. This evidence suggests that the oxidative Cr cycle in terrestrial settings had emerged before the late Ediacaran, but the ^{53}Cr-enriched Cr(VI) species could not affect the deep ocean because of widespread anoxia; thus, the deep ocean retained its low δ^{53}Cr values until the late Ediacaran. Within Stage III (above 80 m), the detrital phases likely have negative δ^{53}Cr values (approximately $\leq \sim -0.1$‰), and the δ^{53}Cr of contemporaneous deep water shows a slight rise to ~0.08‰. If the δ^{53}Cr rise and its amplitude can be confirmed, this would suggest that ^{53}Cr-enriched Cr(VI) species in the surface ocean had begun to affect the deep ocean, implying an oxidation of the ocean in the Huanan basin around the Ediacaran–Cambrian boundary.

Acknowledgments

This research is supported by the Natural Science Foundation of China (41673002, 41625013, 41721002, 41520104007, 41330102, 41373077, 41372003, 41571130052), and the 111 Project to Y. Shen. We thank Dr. J. Wang, Dr. L. Feng and the three anonymous reviewers for field work and constructive comments. We also thank Mary Horan and Tim Mock for laboratory assistance at the Department of Terrestrial Magnetism (DTM) of the Carnegie Institution for Science.

References

Böning, P., Brumsack, H.-J., Böttcher, M.E., Schnetger, B., Kriete, C., Kallmeyer, J., Borchers, S.L., 2004. Geochemistry of Peruvian near-surface sediments. Geochim. Cosmochim. Acta 68, 4429–4451.
Bonnand, P., James, R.H., Parkinson, I.J., Connelly, D.P., Fairchild, I.J., 2013. The chromium isotopic composition of seawater and marine carbonates. Earth Planet. Sci. Lett. 382, 10–20.
Buerge, I.J., Hug, S.J., 1997. Kinetics and pH dependence of Chromium(VI) reduction by Iron(II). Environ. Sci. Technol. 31, 1426–1432.
Canfield, D.E., Poulton, S.W., Knoll, A.H., Narbonne, G.M., Ross, G., Goldberg, T., Strauss, H., 2008. Ferruginous conditions dominated later Neoproterozoic deep-water chemistry. Science 321, 949–952.
Chang, H.J., Chu, X.L., Feng, L.J., Huang, J., 2009. Framboidal pyrites in cherts of the Laobao formation, South China: evidence for anoxic deep ocean in the terminal Ediacaran. Acta Petrol. Sin. 25 (4), 1001–1007 (in Chinese with English abstract).
Chang, H.J., Chu, X.L., Feng, L.J., Huang, J., 2010a. Iron speciation in cherts from the Laobao formation, South China: implications for anoxic and ferruginous deep-water conditions. Chin. Sci. Bull. 55 (27–28), 3189–3196.
Chang, H., Chu, X., Feng, L., Huang, J., Zhang, Q., 2010b. The major and REE geochemistry of the Silikou Chert in Northern Guangxi Province. Acta Sedimentol. Sin. 28, 1098–1107 (in Chinese with English abstract).
Chang, H.-J., Chu, X.-L., Feng, L.-J., Huang, J., 2012. Progressive oxidation of anoxic and ferruginous deep-water during deposition of the terminal Ediacaran Laobao formation in South China. Palaeogeogr. Palaeoclimatol. Palaeoecol. 321–322, 80–87.
Chen, D.Z., Wang, J.G., Qing, H.R., Yan, D.T., Li, R.W., 2009. Hydrothermal venting activities in the Early Cambrian South China: petrological, geochronological and stable isotopic constraints. Chem. Geol. 258, 168–181.
Chen, D., Zhou, X., Fu, Y., Wang, J., Yan, D., 2015a. New U–Pb zircon ages of the Ediacaran–Cambrian boundary strata in South China. Terra Nova 27, 62–68.
Chen, X., Ling, H.-F., Vance, D., Shields-Zhou, G.A., Zhu, M., Poulton, S.W., Och, L.M., Jiang, S.-Y., Li, D., Cremonese, L., Archer, C., 2015b. Rise to modern levels of ocean oxygenation coincided with the Cambrian radiation of animals. Nat. Commun. 6, 7142. http://dx.doi.org/10.1038/ncomms8142.
Condon, D., Zhu, M.Y., Bowring, S., Wang, W., Yang, A.H., Jin, Y.G., 2005. U-Pb ages from the Neoproterozoic Doushantuo formation, China. Science 308, 95–98.
Crowe, S.A., Dossing, L.N., Beukes, N.J., Bau, M., Kruger, S.J., Frei, R., Canfield, D.E., 2013. Atmospheric oxygenation three billion years ago. Nature 501, 535–538.
Dong, L., Shen, B., Lee, C.-T.A., Shu, X.J., Peng, Y., Sun, Y., Tang, Z., Rong, H., Lang, X., Ma, H., Yang, F., Guo, W., 2015. Germanium/silicon of the Ediacaran-Cambrian Laobao cherts: implications for the bedded chert formation and paleoenvironment interpretations. Geochem. Geophys. Geosyst. 16, 751–763.
Eary, L.E., Rai, D., 1989. Kinetics of chromate reduction by ferrous ions derived from hematite and biotite at 25 °C. Am. J. Sci. 289, 180–213.
Edmonds, H.N., German, C.R., 2004. Particle geochemistry in the rainbow hydrothermal plume, Mid-Atlantic Ridge1. Geochim. Cosmochim. Acta 68, 759–772.
Erwin, D.H., Laflamme, M., Tweedt, S.M., Sperling, E.A., Pisani, D., Peterson, K.J., 2011. The Cambrian conundrum: early divergence and later ecological success in the early history of animals. Science 334, 1091–1097.
Fan, H., Wen, H., Zhu, X., Hua, R., Tian, S., 2013. Hydrothermal activity during Ediacaran–Cambrian transition: silicon isotopic evidence. Precambrian Res. 224, 23–35.
Fandeur, D., Juillot, F., Morin, G., Olivi, L., Cognigni, A., Ambrosi, J.-P., Guyot, F., Fritsch, E., 2009. Synchrotron-based speciation of chromium in an Oxisol from New Caledonia: importance of secondary Fe-oxyhydroxides. Am. Mineral. 94, 710–719.
Farkaš, J., Chrastný, V., Novák, M., Čadkova, E., Pašava, J., Chakrabarti, R., Jacobsen, S.B., Ackerman, L., Bullen, T.D., 2013. Chromium isotope variations ($\delta^{53/52}$Cr) in mantle-derived sources and their weathering products: implications for environmental studies and the evolution of $\delta^{53/52}$Cr in the Earth's mantle over geologic time. Geochim. Cosmochim. Acta 123, 74–92.
Fendorf, S.E., Li, G., 1996. Kinetics of chromate reduction by ferrous iron. Environ. Sci. Technol. 30, 1614–1617.
Fendorf, S.E., Lamble, G.M., Stapleton, M.G., Kelley, M.J., Sparks, D.L., 1994. Mechanisms of Chromium(III) sorption on silica. 1. Chromium(III) surface structure derived by extended X-ray absorption fine structure spectroscopy. Environ. Sci. Technol. 28 (2), 284–289.
Feng, L., Li, C., Huang, J., Chang, H., Chu, X., 2014. A sulfate control on marine mid-depth euxinia on the early Cambrian (ca. 529–521 Ma) Yangtze platform, South China. Precambrian Res. 246, 123–133.
Fike, D.A., Grotzinger, J.P., Pratt, L.M., Summons, R.E., 2006. Oxidation of the Ediacaran Ocean. Nature 444, 744–747.
Frei, R., Gaucher, C., Poulton, S.W., Canfield, D.E., 2009. Fluctuations in Precambrian atmospheric oxygenation recorded by chromium isotopes. Nature 461, 250–253.
Frei, R., Gaucher, C., Døssing, L.N., Sial, A.N., 2011. Chromium isotopes in carbonates — a tracer for climate change and for reconstructing the redox state of ancient seawater. Earth Planet. Sci. Lett. 312, 114–125.
Frei, R., Gaucher, C., Stolper, D., Canfield, D.E., 2013. Fluctuations in late Neoproterozoic atmospheric oxidation — Cr isotope chemostratigraphy and iron speciation of the late Ediacaran lower Arroyo del Soldado Group (Uruguay). Gondwana Res. 23, 797–811.
Frei, R., Poiré, D., Frei, K.M., 2014. Weathering on land and transport of chromium to the ocean in a subtropical region (Misiones, NW Argentina): a chromium stable isotope perspective. Chem. Geol. 381, 110–124.
German, C.R., Klinkhammer, G.P., Edmond, J.M., Mitra, A., Elderfield, H., 1990. Hydrothermal scavenging of rare-earth elements in the ocean. Nature 345, 516–518.
German, C.R., Holliday, B.P., Elderfield, H., 1991. Redox cycling of rare earth elements in

the suboxic zone of the Black Sea. Geochim. Cosmochim. Acta 55, 3553–3558.
Gilleaudeau, G.J., Frei, R., Kaufman, A.J., Kah, L.C., Azmy, K., Bartley, J.K., Chernyavskiy, P., Knoll, A.H., 2016. Oxygenation of the mid-Proterozoic atmosphere: clues from chromium isotopes in carbonates. Geochemical Perspectives Letters 2, 178–187.
Gueguen, B., Reinhard, C.T., Algeo, T.J., Peterson, L.C., Nielsen, S.G., Wang, X., Rowe, H., Planavsky, N.J., 2016. The chromium isotope composition of reducing and oxic marine sediments. Geochim. Cosmochim. Acta 184, 1–19.
Han, R., Qin, L., Brown, S.T., Christensen, J.N., Beller, H.R., 2012. Differential isotopic fractionation during Cr(VI) reduction by an aquifer-derived bacterium under aerobic versus denitrifying conditions. Appl. Environ. Microbiol. 78, 2462–2464.
Holmden, C., Jacobson, A., Sageman, B., Hurtgen, M., 2016. Response of the Cr isotope proxy to cretaceous ocean anoxic event 2 in a pelagic carbonate succession from the western interior seaway. Geochim. Cosmochim. Acta 186, 277–295.
Hu, J., 2008. The cherty microbolity in the deeper water facies during the Precambrian–Cambrian transitional period in Northeast Guangxi Province, China. Acta Micropalaeontologica Sinica 25, 291–305 (in Chinese with English abstract).
Jiang, G., Sohl, L.E., Christie-Blick, N., 2003. Neoproterozoic stratigraphic comparison of the lesser Himalaya (India) and Yangtze block (south China): Paleogeographic implications. Geology 31, 917–920.
Konhauser, K., Lalonde, S., Planavsky, N., Pecoits, E., Lyons, T., Mojzsis, S., Rouxel, O., Barley, M., Rosìere, C., Fralick, P., Kump, L., Bekker, A., 2011. Aerobic bacterial pyrite oxidation and acid rock drainage during the great oxidation event. Nature 478, 369–373.
Kotaś, J., Stasicka, Z., 2000. Chromium occurrence in the environment and methods of its speciation. Environ. Pollut. 107, 263–283.
Lawrence, M., Greig, A., Collerson, K., Kamber, B., 2006. Rare earth element and yttrium variability in South East Queensland waterways. Aquat. Geochem. 12, 39–72.
Lehmann, B., Frei, R., Xu, L., Mao, J., 2016. Early Cambrian black shale-hosted Mo-Ni and V mineralization on the rifted margin of the Yangtze platform, China: reconnaissance chromium isotope data and a refined metallogenic model. Econ. Geol. 111, 89–103.
Li, C., Love, G.D., Lyons, T.W., Fike, D.A., Sessions, A.L., Chu, X., 2010. A stratified redox model for the Ediacaran ocean. Science 328, 80–83.
Maloof, A.C., Porter, S.M., Moore, J.L., Dudás, F.Ö., Bowring, S.A., Higgins, J.A., Fike, D.A., Eddy, M.P., 2010. The earliest Cambrian record of animals and ocean geochemical change. Geol. Soc. Am. Bull. 122, 1731–1774.
Marshall, C.R., 2006. Explaining the Cambrian “explosion” of animals. Annu. Rev. Earth Planet. Sci. 34, 355–384.
McFadden, K.A., Huang, J., Chu, X., Jiang, G., Kaufman, A.J., Zhou, C., Yuan, X., Xiao, S., 2008. Pulsed oxidation and biological evolution in the Ediacaran Doushantuo formation. Proc. Natl. Acad. Sci. 105, 3197–3202.
McLennan, S.M., 1989. Rare earth elements in sedimentary rocks; influence of provenance and sedimentary processes. Rev. Mineral. Geochem. 21, 169–200.
Och, L.M., Shields-Zhou, G.A., 2012. The Neoproterozoic oxygenation event: environmental perturbations and biogeochemical cycling. Earth Sci. Rev. 110, 26–57.
Och, L.M., Shields-Zhou, G.A., Poulton, S.W., Manning, C., Thirlwall, M.F., Li, D., Chen, X., Ling, H., Osborn, T., Cremonese, L., 2013. Redox changes in early Cambrian black shales at Xiaotan section, Yunnan Province, South China. Precambrian Res. 225, 166–189.
Oze, C., Bird, D.K., Fendorf, S., 2007. Genesis of hexavalent chromium from natural sources in soil and groundwater. Proc. Natl. Acad. Sci. 104, 6544–6549.
Pattan, J.N., Pearce, N.J.G., Mislankar, P.G., 2005. Constraints in using cerium-anomaly of bulk sediments as an indicator of paleo bottom water redox environment: a case study from the Central Indian Ocean Basin. Chem. Geol. 221, 260–278.
Paulukat, C., Døssing, L.N., Mondal, S.K., Voegelin, A.R., Frei, R., 2015. Oxidative release of chromium from Archean ultramafic rocks, its transport and environmental impact — a Cr isotope perspective on the Sukinda valley ore district (Orissa, India). Appl. Geochem. 59, 125–138.
Paulukat, C., Gilleaudeau, G.J., Chernyavskiy, P., Frei, R., 2016. The Cr-isotope signature of surface seawater — A global perspective. Chem. Geol. 444, 101–109.
Planavsky, N.J., Reinhard, C.T., Wang, X., Thomson, D., McGoldrick, P., Rainbird, R.H., Johnson, T., Fischer, W.W., Lyons, T.W., 2014. Low mid-Proterozoic atmospheric oxygen levels and the delayed rise of animals. Science 346, 635–638.
Qin, L., Wang, X., 2017. Chromium isotope geochemistry. Rev. Mineral. Geochem. 82, 379–414.
Qin, L., Alexander, C.M.O.D., Carlson, R.W., Horan, M.F., Yokoyama, T., 2010. Contributors to chromium isotope variation of meteorites. Geochim. Cosmochim. Acta 74, 1122–1145.
Reinhard, C.T., Planavsky, N.J., Wang, X., Fischer, W.W., Johnson, T.M., Lyons, T.W., 2014. The isotopic composition of authigenic chromium in anoxic marine sediments: a case study from the Cariaco Basin. Earth Planet. Sci. Lett. 407, 9–18.
Rodler, A.S., Hohl, S.V., Guo, Q., Frei, R., 2016. Chromium isotope stratigraphy of Ediacaran cap dolostones, Doushantuo formation, South China. Chem. Geol. 436, 24–34.
Sander, S., Koschinsky, A., 2000. Onboard-ship redox speciation of chromium in diffuse hydrothermal fluids from the North Fiji Basin. Mar. Chem. 71, 83–102.
Scheiderich, K., Amini, M., Holmden, C., Francois, R., 2015. Global variability of chromium isotopes in seawater demonstrated by Pacific, Atlantic, and Arctic Ocean samples. Earth Planet. Sci. Lett. 423, 87–97.
Schijf, J., de Baar, H.J.W., Wijbrans, J.R., Landing, W.M., 1991. Dissolved rare earth elements in the Black Sea. In: Murray, J.W. (Ed.), Black Sea Oceanography—Results from the 1988 Black Sea Expedition, Deep-Sea Research 38, pp. 805–823.
Schoenberg, R., Zink, S., Staubwasser, M., von Blanckenburg, F., 2008. The stable Cr isotope inventory of solid Earth reservoirs determined by double spike MC-ICP-MS. Chem. Geol. 249, 294–306.
Schröder, S., Grotzinger, J.P., 2007. Evidence for anoxia at the Ediacaran–Cambrian boundary: the record of redox-sensitive trace elements and rare earth elements in Oman. J. Geol. Soc. 164, 175–187.
Shen, Y., Zhang, T., Hoffman, P.F., 2008. On the coevolution of Ediacaran oceans and animals. Proc. Natl. Acad. Sci. 105, 7376–7381.
Shen, J., Liu, J., Qin, L., Wang, S.-J., Li, S., Xia, J., Ke, S., Yang, J., 2015. Chromium isotope signature during continental crust subduction recorded in metamorphic rocks. Geochem. Geophys. Geosyst. 16, 3840–3854.
Thompson, C.K., Kah, L.C., 2012. Sulfur isotope evidence for widespread euxinia and a fluctuating oxycline in Early to Middle Ordovician greenhouse oceans. Palaeogeogr. Palaeoclimatol. Palaeoecol. 313-314, 189–214.
Wang, J., Li, Z.-X., 2003. History of Neoproterozoic rift basins in South China: implications for Rodinia break-up. Precambrian Res. 122, 141–158.
Wang, J., Chen, D., Yan, D., Wei, H., Xiang, L., 2012a. Evolution from an anoxic to oxic deep ocean during the Ediacaran–Cambrian transition and implications for bioradiation. Chem. Geol. 306-307, 129–138.
Wang, J., Chen, D., Wang, D., Yan, D., Zhou, X., Wang, Q., 2012b. Petrologyand geochemistry of chert on the marginal zone of Yangtze platform, Western Hunan, South China, during the Ediacaran–Cambrian transition. Sedimentology 59, 809–829.
Wang, X., Shi, X., Jiang, G., Zhang, W., 2012c. New U–Pb age from the basal Niutitang formation in South China: implications for diachronous development and condensation of stratigraphic units across the Yangtze platform at the Ediacaran–Cambrian transition. J. Asian Earth Sci. 48, 1–8.
Wang, X., Planavsky, N., Reinhard, C., Zou, H., Ague, J., Wu, Y., Gill, B., Schwarzenbach, E., Peucker-Ehrenbrink, B., 2016. Chromium isotope fractionation during subduction-related metamorphism, black shale weathering, and hydrothermal alteration. Chem. Geol. 423, 19–33.
Wen, H., Fan, H., Zhang, Y., Cloquet, C., Carignan, J., 2015. Reconstruction of early Cambrian ocean chemistry from Mo isotopes. Geochim. Cosmochim. Acta 164, 1–16.
Wilkin, R.T., Barnes, H.L., Brantley, S.L., 1996. The size distribution of framboidal pyrite in modern sediments: an indicator of redox conditions. Geochim. Cosmochim. Acta 60 (20), 3897–3912.
Wilkin, R.T., Arthur, M.A., Dean, W.E., 1997. History of water-column anoxia in the Black Sea indicated by pyrite framboid size distributions. Earth Planet. Sci. Lett. 148, 517–525.
Wille, M., Nagler, T.F., Lehmann, B., Schroder, S., Kramers, J.D., 2008. Hydrogen sulphide release to surface waters at the Precambrian/Cambrian boundary. Nature 453, 767–769.
Zhang, X., Shu, D., 2014. Causes and consequences of the Cambrian explosion. Sci. China Earth Sci. 57, 930–942.
Zhu, M., Zhang, J., Yang, A., 2007. Integrated Ediacaran (Sinian) chronostratigraphy of South China. Palaeogeogr. Palaeoclimatol. Palaeoecol. 254, 7–61.
Zink, S., Schoenberg, R., Staubwasser, M., 2010. Isotopic fractionation and reaction kinetics between Cr(III) and Cr(VI) in aqueous media. Geochim. Cosmochim. Acta 74, 5729–5745.